A&A 532, A104 (2011)
DOI: 10.1051/0004-6361/201016004

Astronomy & Astrophysics

Hubble flow around Fornax cluster of galaxies★

O. G. Nasonova[1,2,★★], J. A. de Freitas Pacheco[1], and I. D. Karachentsev[2,3]

[1] Université de Nice – Sophia Antipolis, Observatoire de la Côte d'Azur Laboratoire Cassiopée, UMR 6202, BP-4229, 06304 Nice Cedex 4, France
e-mail: phiruzi@gmail.com
[2] Special Astrophysical Observatory of the Russian Academy of Sciences Laboratory of Extragalactic Astrophysics and Cosmology Nizhnij Arkhyz, 369167, Karachay-Cherkessia, Russia
[3] Université de Lyon, Université Lyon 1, CNRS/IN2P3, Institut de Physique Nucléaire de Lyon, 69622 Villeurbanne, France

Received 26 October 2010 / Accepted 1 June 2011

ABSTRACT

Aims. This work aims to provide a new mass estimate for the Fornax cluster and the Fornax-Eridanus complex, avoiding methods like the virial or fits of the X-ray emission profile, which assume that the system is in equilibrium. This is probably not the case for Fornax, because it is still in process of formation.

Methods. Our mass estimate is based on determination of the zero-velocity surface, which, in the context of the spherical infall model, permits an evaluation of the total mass inside such a surface. The zero-velocity surface radius R_0 was estimated either by a running median procedure or by fitting the data to the velocity field expected from the spherical model, including effects of the cosmological constant. The velocity field in a region within 20 Mpc of the Fornax center was mapped using a list of 109 galaxies whose distances have an average accuracy of 0.31 mag in their distance modulus.

Results. Our analysis indicates that the mass of the Fornax cluster itself is $[0.40-3.32] \times 10^{14}$ $M_\odot$ inside a radius of [2.62−5.18] Mpc while the mass inside [3.88−5.60] Mpc, corresponding to the Fornax-Eridanus complex, is $[1.30-3.93] \times 10^{14}$ $M_\odot$.

Key words. galaxies: clusters: individual: Fornax

1. Introduction

In the hierarchical scenario of structure formation, clusters of galaxies are one of the largest structures observed in nature. Clusters have been assembled relatively late in the history of the universe, since they are located in the intersection of filaments that constitute the cosmic web (Voit 2005). Clusters are bound essentially by the gravitational action of so-called dark matter, while the luminous (baryonic) component gives only a minor contribution to the gravitational potential of the system. Moreover, most of the baryonic matter is in the form of hot and warm gas filling the intracluster medium, which is detected by its X-ray emission. Clusters of galaxies are of particular interest in cosmology since the evolution of their number density above a given mass provide strong constraints on parameters characterizing different world models (Rosati et al. 2002).

Masses of clusters are generally estimated by using the virial relation, which presupposes that the system is dynamically relaxed. This is not the case during phases in which the cluster undergoes a merger episode or accretes mass through filaments (see, for instance, Girardi & Biviano 2002). Moreover, this method is affected by the eventual inclusion of interlopers by projection effects in the considered sample and by dynamical friction, which may introduce strong bias between the velocity dispersion of galaxies and dark matter particles. The reliability of the virial relation as a mass estimator has been checked by numerical simulations performed by different authors. Danese et al. (1981) and Fernley & Bhavsar (1984) concluded that projection effects are important because they may considerably affect the virial masses. Similar results were obtained by Perea et al. (1990), who reached the conclusion that the virial, in general, overestimates the masses unless interlopers are eliminated. A more recent study by Biviano et al. (2006) has led to more quantitative results: the virial relation overestimates true masses by about 10% if the simulated clusters have more than 60 members, with uncertainties increasing up to 50–60% for objects having 15–20 members.

Besides the virial, other methods have been frequently employed as mass estimators of clusters. The X-ray emission profile of the hot intracluster gas can be used to trace the gravitational potential of clusters, under the assumption of hydrostatic equilibrium (Sarazin 1986; Reiprich & Bohringer 2002). The accuracy of this approach was tested by cosmological simulations, which indicate that when masses are evaluated inside a radius at which the mean cluster density is about 500–2500 times the critical density, the uncertainties range from 14 to 29% (Evrard et al. 2006). The masses of galaxy clusters can also be estimated through analyzing of gravitational lensing, since the gravitational field of clusters distorts the image of galaxies situated behind them (Broadhurst et al. 1995). A comparison of masses resulting from X-ray data and strong lensing shows that values drawn from the latter method are, on the average, twice those obtained from the former procedure (Wu 2000). These differences could be the consequence of an oversimplification of the lens model and/or violation of the hypothesis of gas isothermality. More recently, weak gravitational lensing, a technique

★ The catalog is only available in electronic form at the CDS via anonymous ftp to cdsarc.u-strasbg.fr (130.79.128.5) or via http://cdsarc.u-strasbg.fr/viz-bin/qcat?J/A+A/532/A104
★★ Née Kashibadze.

permitting tracking of the gravitational potential of these objects by the distortion induced in the shape of background galaxies (see, for instance, Mellier 1999) has been used to estimate masses of different clusters. However, the presence of nearby filaments leads in general to overestimating masses by 10–30% (Metzler et al. 1999).

All the above-mentioned methods correspond to scales less than or close to 1–2 Mpc, which are typical dimensions for the central region of galaxy clusters. On larger scales, corresponding to the surroundings of clusters, galaxies are probably falling onto the cluster for the first time. Despite of being bound to the cluster, these outskirt galaxies are not in dynamical equilibrium. In this case, the knowledge of the velocity field of these objects may lead to an estimate of the central region's mass. In fact, such an approach has been proposed by Lynden-Bell (1981) and Sandage (1986) based on the spherical infall model. The motion of the outskirt galaxies is supposed to be radial and the mass inside such a surface can be estimated from the knowledge of the distance R_0, at which the radial velocity with respect to the center of mass is zero. The spherical model also predicts the existence of caustics, surfaces at which (theoretically) the galaxy number density is infinite (Regos & Geller 1989). The profile of the caustic amplitude, as seen in a phase-space diagram for the outskirt galaxies, can be used as a mass estimator with an accuracy of a factor of two (Diaferio 1999).

In the present paper we intend to present a new estimate of the mass of the southern cluster located in Fornax (Abell S0373) at a distance of 20 Mpc. An early survey in the Fornax area performed by Ferguson (1989) indicates that probably 340 galaxies are cluster members, and a fit of the projected density with a King profile suggests a core radius of about 0.7°. Despite of being less rich than Virgo, this system presents different interesting features. Its main structure is centered on NGC 1399. According to Drinkwater et al. (2001), dwarf galaxies form a distinct population that is probably falling into the main system. Using the method by Diaferio (1999) mentioned above, which does not assume dynamical equilibrium, Drinkwater et al. (2001) estimate the projected mass inside a radius of 1.4 Mpc as $(7\pm2)\times10^{13}\ M_{\odot}$. Since then a large amount of data on galaxies within the Local Universe, including radial velocities and precise distances, has been accumulated. This justifies a novel study of the velocity field in the Fornax region, as well as new estimates of its mass, based on the analysis of the velocity field of outskirt galaxies, modeled by the spherical infall model and avoiding problems found in other mass indicators as mentioned above. This paper is organized as follows. In Sect. 2 the available data is presented, mass estimates are discussed in Sect. 3, and finally the main results are summarized in Sect. 4.

2. The data

In the past decade a significant number of galaxies present in the Local Volume had their distances measured with quite good accuracy, in particular thanks to data obtained with the Hubble Space Telescope (Karachentsev et al. 2002a,b, 2006, 2009). A substantial effort was also made to increase the database on the Virgo cluster, along with galaxies present in the neighborhood of the Local Group.

Distances to galaxies in the Local Universe have been estimated from different methods:

1) TRGB, based on the luminosity of the tip of the Red Giant Branch, considered as one of the most efficient methods for determining the distances of nearby galaxies, practically independent of their morphological type. The method requires images in two or more photometric bands obtained with WFPC2 or ACS cameras onboard the HST and yields an accuracy of about 7% on distances when derived by such a procedure (Rizzi et al. 2007). A consolidated list of distances for galaxies in the Local Volume is given in the *Catalog of Neighboring Galaxies* (hereafter CNG, Karachentsev et al. 2004). Galaxies from CNG with only TRGB or Cepheid distances were used, including some new determinations (Karachentsev et al. 2006; Tully et al. 2006);
2) the surface brightness fluctuation method (SBF), when applied to early type galaxies, assumes that the old stellar population present in those objects makes the main contribution to their luminosity. The method presupposes that the brightness distribution is not affected by irregularities like the one introduced by the presence of dust clouds. Using this approach, Tonry et al. (2001) determined SBF distances for 300 E and S0 galaxies with typical errors of ∼12%. Galaxies in this sample are distributed over the whole sky, extend up to cz ∼4000 km s^{-1}, and have a median velocity of ∼1800 km s^{-1};
3) Blakeslee et al. (2009) undertook a two-color ACS/HST imaging survey including 43 early type galaxies situated in the Fornax core (the ACS Fornax Cluster Survey project, hereafter ACS-FCS), deriving SBF distances with errors of about 8%. To the ACS-FCS list were added 18 dwarf ellipticals belonging to the cluster, having SBF distances with an accuracy of about 9% estimated by Jerjen (2003) and Dunn & Jerjen (2006). These authors suggest from the S-shaped pattern distribution of these galaxies that Fornax is still in the process of formation;
4) two galaxies within 15 Mpc of the Fornax cluster with distances measured with an accuracy of 5% by using SNIa light curves (Tonry et al. 2003) were also included in our database;
5) Kashibadze (2008) determined distances for 402 edge-on spiral galaxies selected from the *2MASS Flat Galaxy Catalog* (2MFGC, Mitronova et al. 2004), having radial velocities less than 3000 km s^{-1}. Using a multiparametric NIR Tully-Fisher relation, distances with an accuracy of about 20% were obtained. The zero point of the *luminosity-line width* relation was established by using 15 galaxies with distances derived from cepheids and TRGB data;
6) we supplemented the aforementioned samples with a compilation of distances by Tully et al. (2008, 2009) derived from the Tully-Fisher relation calibrated for optical (B, V, R, I) magnitudes. This compilation relies on numerous HI line and photometric observations carried out by Methewson & Ford (1996), Haynes et al. (1999), Tully & Pierce (2000), Koribalski et al. (2004), Springob et al. (2005), Theureau et al. (2006), and other authors. Again, the zero point of these relations were set by using a sample of 40 galaxies with distances determined by cepheids and TRGB data. Finally, the list of galaxies by Springob et al. (2007) (SFI++ sample), not considered by Tully et al. (2009), was also used in our compilation.

The first four samples are referred to as *precise data* because their typical errors do not exceed 10–12%, while the last two datasets are mentioned as *Tully-Fisher data*.

In this paper we generally follow Karachentsev & Nasonova (2010) and examine the *3D sample* to consider galaxies with limited spatial distances from the Fornax cluster center. As discussed by the authors, this approach is not free of systematical effects because galaxy distances are measured with errors, and

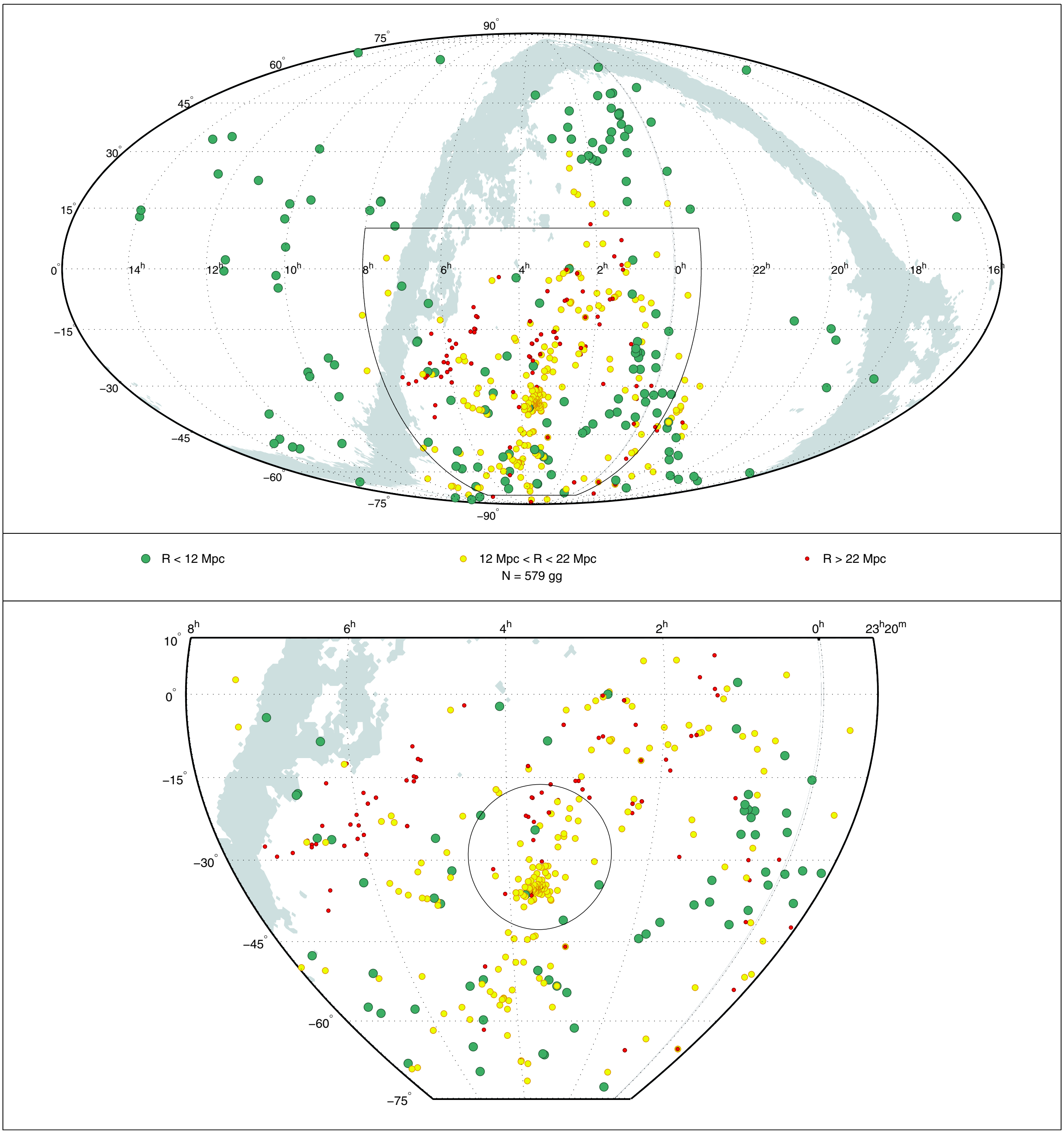

Fig. 1. Sky distribution in equatorial coordinates of 562 galaxies within 20 Mpc from the Fornax center. Markers of different diameters indicate three distinct distance ranges from the Local Group. The circle in the lower panel corresponds to the zero velocity sphere projection (R_0 = 4.60 Mpc) for the Fornax-Eridanus complex.

their significance is different at the proximate and the distant boundary of the spherical volume (the so-called Malmquist bias; see Fig. 2).

Our initial list includes 1140 galaxies within 30 Mpc of the Fornax cluster (the catalog is available at the CDS). However, in the present study, we focus on a region of 20 Mpc around the center of the cluster, representing a sample of 562 objects which, in principle, would permit an estimate not only of zero velocity surface but also of the transition region between bound and unbound objects, the latter essentially tracking the Hubble flow. The characteristics of these galaxies are given in Table 1. The first column indicates the distance estimate method, the second column the mean error in the distance modulus, the third column the number of galaxies, and the last column gives the sample goodness defined as $G = (N/100)^{1/2}\sigma_{\rm m}^{-1}$ (Kudrya et al. 2003). Figure 1 shows the projected distribution of these galaxies in the sky. Galaxies are marked as circles and their diameters indicate different distance ranges.

2.1. The velocity field

In order to map the velocity field around the Fornax center and to have an estimate of the *velocity-distance* relation, accurate radial velocities and distances are required. Then, in the next step, these

Table 1. Database for galaxies within 20 Mpc from the Fornax center.

Distance method	σ_m	N	G
TRGB + Ceph	0.15	113	7.1
SBF (Tonry)	0.25	69	3.3
ACSFCS+	0.19	55	3.9
SNIa (Tonry)	0.10	2	1.4
TF (IR)	0.40	69	2.1
TF (opt)	0.40	254	4.0
All	–	562	27.8

data must be converted into distances and velocities relative to the cluster center.

Data on radial velocities, mostly from HI observations, were obtained in most cases from the same sources of distances. When not available, NED data on heliocentric velocities were used. Observational errors in radial velocities are quite small (1–2 km s^{-1}) in the case of HI observations (Tifft & Huchtmeier 1990) and can be neglected in comparison with distance errors ($\Delta V \ll \Delta R H_0$) on the scales of the nearest clusters ($R \gtrsim$ 15 Mpc).

The transformation of heliocentric velocities into the Local Group reference frame was performed with the standard apex parameters (Karachentsev & Makarov 1996) adopted in NED. If φ is the angular separation between the apex and a galaxy, then the converted velocity is $V_{\rm con} = V + V_{\rm apex} \cos\varphi$ and the error of this conversion is not more than $\left[(\Delta V)^2 + (\Delta V_{\rm apex})^2 + (\Delta\varphi V_{\rm apex})^2\right]^{1/2}$, where $\Delta V_{\rm apex} = 5$ km s^{-1} and $\varphi \approx 1\%$, so $\Delta\varphi V_{\rm apex} \approx 3$ km s^{-1}. Thus, the errors introduced by this transformation are about 6 km s^{-1}, which are negligible in comparison with distance errors.

The gravitational effect of the Fornax cluster can be seen directly from the radial velocity vs. distance relation as an S-shaped wave. Radial velocities and distances relative to the Local Group centroid for 98 galaxies in the cluster core ($\theta < 5°$) are represented in the top panel of Fig. 2. Here, precise distances for most galaxies were obtained within the special survey ACS-FCS with HST (Blakeslee et al. 2009). The centroid of galaxies forming the "virial column" at [19.58 ± 1.25] Mpc is marked in (see Sect. 3.1 for discussion of the Fornax cluster barycenter position). The plotted value of virial radius, ±1.25 Mpc, is an approximate estimate based on the R_0 value for the Fornax-Eridanus complex obtained in this paper (4.60 Mpc). The S-shaped curves correspond to masses of 1.30×10^{14} $M_\odot$ and 3.93×10^{14} $M_\odot$ (see Sect. 3.2 for details). The typical distance error bars for datasets (2), (3) and (4) are shown.

The distribution of radial velocities and distances for the remaining galaxies of the sample at the periphery of the Fornax cluster ($5° < \theta < 30°$) is shown in the bottom panel of Fig. 2. Here, the S-shaped lines having lower amplitudes describe the behavior of perturbed Hubble flow at an angular distance of $\theta = 5°$. The typical distance error bars for datasets (1), (6), and (7) are presented.

However, a serious source of uncertainty is caused by the absence of data on tangential velocities. To estimate galaxy velocities with respect to the center of mass of Fornax, some model should be used, so the results turn out to be model-dependent. Considering the lack of data on the true velocity vector of galaxies, there are at least two approaches to obtaining such a transformation.

The first one assumes that the prevailing motion, which involves most of the galaxies under study, is the asymptotic Hubble relationship (the model of the *minor attractor*). The second approach considers that galaxies are within the infall zone (the model of the *major extended attractor*); i.e., they do not follow the Hubble flow but instead are falling towards the cluster center. Both cases were discussed in detail by Karachentsev & Nasonova (2010); see Fig. 3 sketching the relative positions of the considered galaxy (G), the observer (LG), and the cluster center).

When a galaxy is located strictly in front of or behind the cluster center (i.e. the angles λ and θ are small), both approaches yield the same infall velocity toward the cluster center. When λ is close to 90°, in the second case $V_{\rm in} \to \infty$ leads to a significant discrepancy between the two approaches. However, there are no dramatic differences between both methods in the Hubble diagram. Some galaxies move along the vertical axis appreciably, but the behavior of running medians (see next section) traces the infall of galaxies towards the cluster in a similar way. Nevertheless, as we shall see later, the second method systematically yields slightly higher values of R_0. The scatter of galaxies in the Hubble diagram also increases in the second case. These considerations suggest that the first approach should be preferred.

Finally, to reduce the role of the unknown tangential component of the velocity and to avoid further uncertainties, we decided to select only galaxies situated approximately in front and behind the cluster for our analysis, i.e. in a cone satisfying the conditions $\lambda < 45°$ or $\lambda > 135°$. The number of galaxies satisfying this additional constraint within 20 Mpc of the Fornax center is 164, and their projected distribution in the sky is shown in Fig. 4.

It should be mentioned that the role of possible chaotic tangential velocities of the galaxies has been studied by Karachentsev & Kashibadze (2006). They performed numerical simulations and added some random tangential component to the observed radial velocity. Their modeling of the Hubble flow in the vicinity of the Local Group showed that typical tangential velocities with amplitudes of 35 and 70 km s^{-1} produce a statistical uncertainty in the evaluation of the zero-velocity surface radius as small as ±2% and ±4%, respectively.

3. Mass estimates

The difficulties with the different mass estimators have already been mentioned; in particular, the presence of interlopers leads to an overestimate of the mass ranging from 10% up to 60% when the virial relation is used, whereas estimates based on X-ray data have uncertainties ranging from 14–30%.

The case of the Fornax cluster is quite particular. Unlike clusters as Coma or Virgo, which have well-defined centers and a more or less smooth mass distribution, despite the presence of some substructures, the Fornax cluster has a complicated mass distribution, including many substructures. Such a complexity is sketched in Fig. 5 where it is possible to identify the Fornax cluster centered on NGC 1399, the Eridanus subcluster, including the groups NGC 1407, NGC 1332, NGC 1395, and NGC 1398, as well as other small neighboring groups. It should be emphasized that the virial radii of these groups do not overlap, which suggests that these objects are separated and constitute gravitationally bound structures. However, these groups overlap in the scale of the zero-velocity radius, indicating that, despite the absence of dynamical equilibrium, they are probably bound to the main structure.

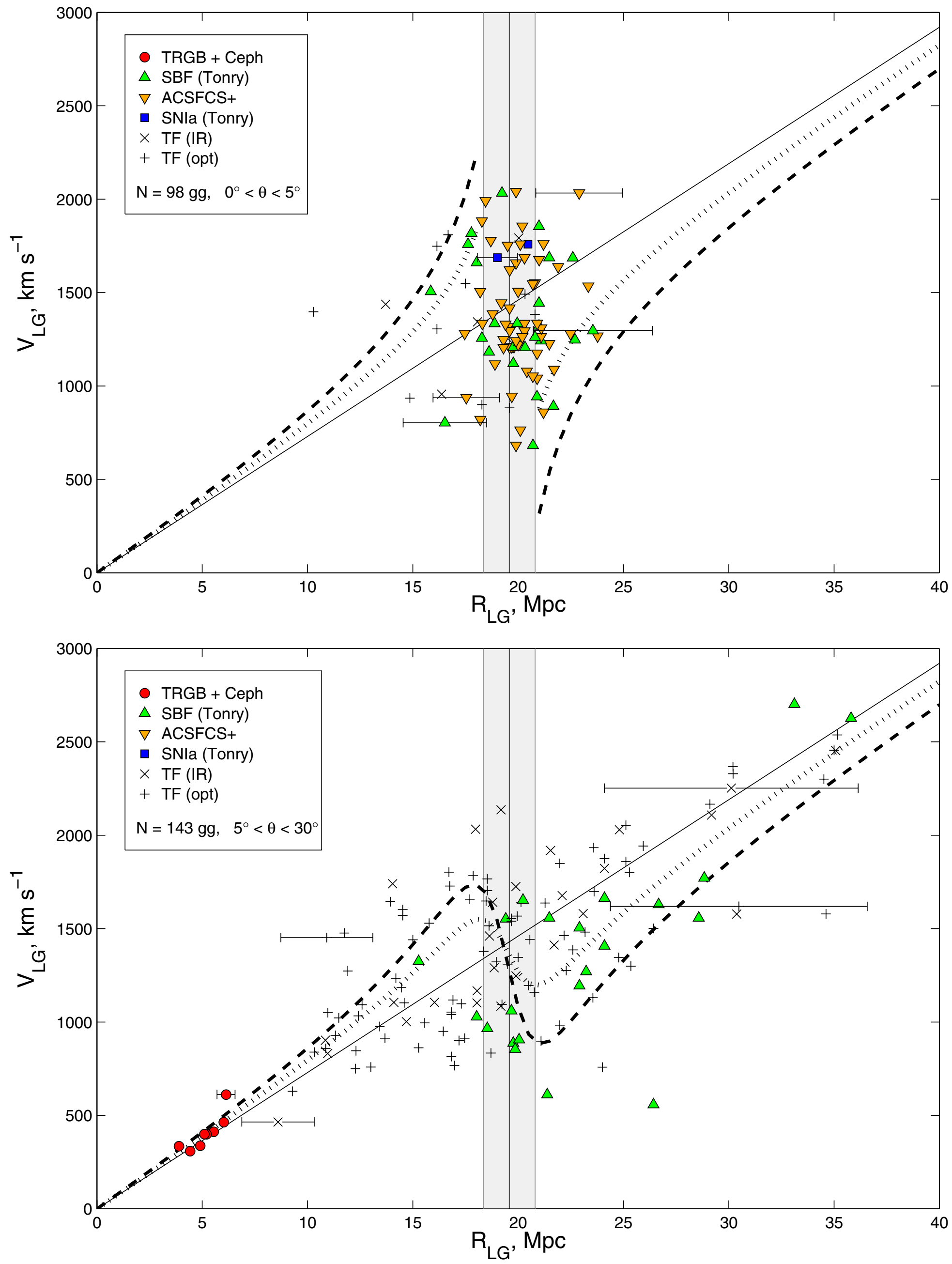

Fig. 2. Radial velocity vs. distance relation for galaxies in the Fornax cluster region with respect to the Local Group centroid. Galaxy samples with distances derived by different methods are marked by different symbols. The inclined straight line traces Hubble relation with the global Hubble parameter H_0 = 73 km s^{-1} Mpc^{-1}. The virial zone is filled with gray. Two S-shaped lines correspond to a Hubble flow perturbed by masses of 1.30×10^{14} $M_{\odot}$ (dotted) and 3.93×10^{14} $M_{\odot}$ (dashed) as the limiting cases within the confidence range in the case of line-of-sight passing exactly through the cluster center. The typical distance error bars for each dataset are shown. *Top*: the cluster core within angular distance $\theta < 5°$, the S-shaped lines indicate the expected infall at $\theta = 0°$. *Bottom*: peripheric regions with $5° < \theta < 30°$, the S-shaped lines indicates the infall at $\theta = 5°$.

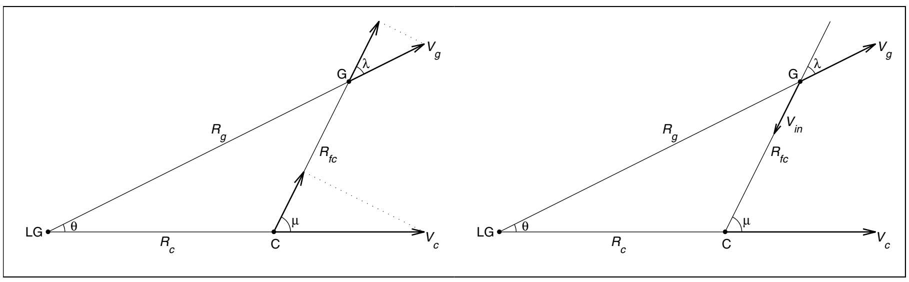

Fig. 3. Relative positions between the observer *LG*, the considered galaxy *G* and the cluster center *C*. *Left panel*: case of a pure Hubble flow. *Right panel*: case of a pure infall towards the Fornax center.

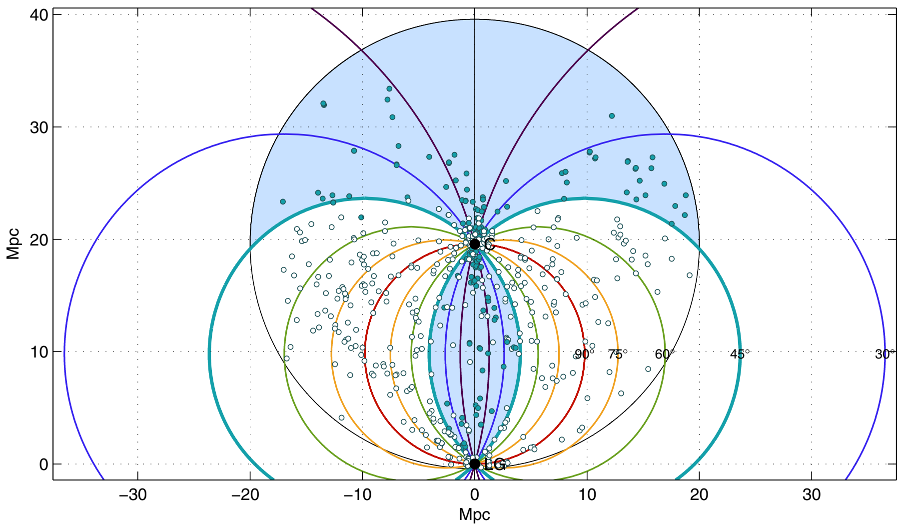

Fig. 4. Spatial distribution of galaxies around the Fornax cluster. The zones where $\lambda < 45°$ or $\lambda > 135°$ are shaded blue whereas the exclusion zones are white. The same color code indicates if galaxies are included in the analysis. For clarity, lines of equal λ for values in the range 15°–90° are also shown.

Table 2. Groups, triplets, and pairs around the Fornax-Eridanus complex with individual distances.

Group	RA, Dec	N	N_D	V_{LG}	±	σ_v	R_h	lg L_K	lg M	D	±	D_h	θ	λ	θ'	λ'
	hh mm ss dd mm ss			km s^{-1}		km s^{-1}	kpc	$L_\odot$	$M_\odot$	Mpc		Mpc	°	°	°	°
(1)	(2)	(3)	(4)	(5)	(6)	(7)	(8)	(9)	(10)	(11)	(12)	(13)	(14)	(15)	(16)	(17)
NGC 1097	024621.0−314430	4	1	1189	81	140	43	11.26	12.53	15.9	3.2	16.3	11	131	10	142
NGC 1187	030238.6−230819	4	1	1315	28	48	106	10.60	11.90	18.4	3.7	18.0	15	96	9	125
NGC 1201	030408.0−275549	2	2	1633	48	48	312	10.95	11.94	21.0	0.8	22.4	12	65	7	88
NGC 1232	030945.5−212514	3	2	1582	49	70	475	11.07	12.93	19.2	0.5	21.7	16	86	10	113
NGC 1291	031718.6−425331	3	3	703	70	99	226	11.03	13.09	8.2	0.5	9.6	6	170	13	159
NGC 1302	031723.8−260702	6	4	1663	21	47	383	11.15	12.30	19.2	1.0	22.8	10	91	5	136
NGC 1332	032500.7−212102	22	9	1469	40	183	279	11.55	13.39	24.1	0.8	20.1	15	45	8	43
NGC 1340	032819.7−325555	3	2	1074	4	6	432	10.73	11.76	20.2	0.4	14.7	5	67	3	131
NGC 1399	033230.3−360845	111	79	1411	23	244	454	12.30	13.94	19.6	0.2	19.3	0	0	7	116
IC 1970	033631.5−440235	2	1	1090	9	9	103	10.06	10.06	19.4	2.0	14.9	8	90	15	99
NGC 1386	033734.3−360610	8	5	755	26	70	165	10.37	12.40	19.8	0.9	10.3	1	58	7	113
NGC 1398	033754.9−260905	10	4	1386	30	89	612	11.46	13.09	22.7	1.8	19.0	10	45	3	34
NGC 1407	034002.6−191705	25	5	1713	34	167	385	11.61	13.22	24.2	1.2	23.5	17	47	10	47
NGC 1395	034014.0−231718	24	11	1548	25	121	378	11.53	13.05	24.3	1.0	21.2	13	41	6	34
NGC 1482	035438.9−212951	3	2	1715	55	78	48	10.70	11.32	28.9	3.1	23.5	16	28	9	23
NGC 1519	040703.1−183633	4	2	1781	15	26	238	10.29	11.57	23.8	2.4	24.4	20	51	14	56
NGC 1532	041226.4−332640	10	3	1159	30	89	137	11.25	12.70	20.3	1.5	15.9	9	72	9	98

3.1. The spatial position of the Fornax-Eridanus barycenter

In the present paper we regard the dynamical center of the Fornax cluster (NGC 1399 group) situated near the core of the hot X-ray emitting gas (Jones et al. 1997; Scharf et al. 2005; Machacek et al. 2005) as the gravity center of the whole Fornax-Eridanus complex. Its spatial position was calculated as the mean position of all NGC 1399 group members, yielding $D = 19.6$ Mpc, $\alpha = 3^{\rm h}32^{\rm m}30^{\rm s}$ and $\delta = -35°51'15''$. For the moment this choice (as the first approximation) seems to be reasonable since the NGC 1399 region has been investigated in the most detail. The next step is to determine the spatial position of the Fornax-Eridanus complex barycenter as the weighted mean for position vectors of all the virialized substructures forming the complex. This will be possible after obtaining more observational data in a wider area of the complex. Still, the same calculation techniques we applied for both center positions (with values $R = 21.1$ Mpc, $\alpha = 3^{\rm h}33^{\rm m}58^{\rm s}$, $\delta = -28°44'45''$ adopted for the second case), and the resulting R_0 values do not differ significantly. The barycenter position associated with NGC 1399 group yields 0.23 Mpc lower R_0 value from precise data and 0.19 Mpc higher value from Tully-Fisher data, leading to the upper bound of discrepancy ~0.2 Mpc. Generally speaking, the zero-velocity surface method is rather stable in the sense of a barycenter position (Karachentsev & Kashibadze 2006).

Table 2 represents the groups, triplets, and pairs that form the Fornax-Eridanus complex with individual distance estimates (Karachentsev & Makarov 2008; Makarov & Karachentsev 2009, 2011). Columns of the table contain: (1) name of the brightest galaxy in a group/triplet/pair; (2) equatorial coordinates of the brightest galaxy for triplets and pairs or mean equatorial coordinates for groups (at the J2000.0 equinox); (3) number of galaxies in a system; (4) number of galaxies with measured distances; (5, 6) mean velocity with respect to the Local Group centroid and its error; (7) radial velocity dispersion; (8) harmonical radius; (9) integrated luminosity of the group in the K_s band; (10) virial mass of the group; (11, 12) mean distance of the group and its error; (13) *Hubble distance* calculated as $D_h = H_0 V_{LG}$ where $H_0 = 73$ km s^{-1} Mpc^{-1}; (14) and (16) angular distance to the Fornax-Eridanus complex barycenter for the cases of (14) dynamical center of the NGC 1399 group situated near the center of the hot X-ray emitting gas and (16) dynamical center of all substructures forming the complex; (15) and (17) angle between the directions to the Local Group and

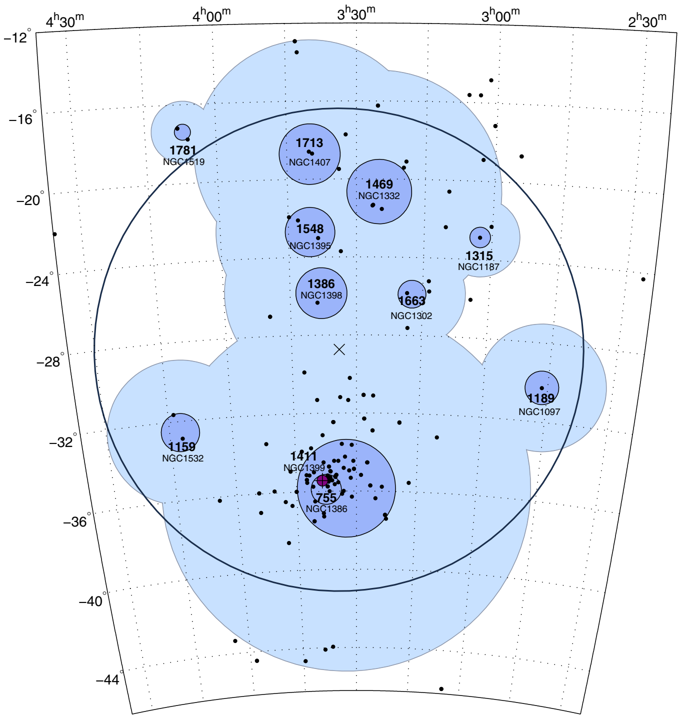

Fig. 5. Fornax cluster (*NGC 1399 group*), Eridanus subcluster (*NGC 1395, NGC 1407, NGC 1332, NGC 1398 groups*) and other neighboring groups of galaxies forming the Fornax complex (Makarov & Karachentsev 2011). On the scales of virial radii (dark-blue circles) these overdensities constitute separate bound groups, but they overlap substantially on scales of R_0 (light-blue regions). The velocities of groups V_{LG} are indicated near the names of their central galaxies. NGC 1399, as the most massive galaxy in the complex situated near the center of the hot X-ray emitting gas, is indicated as a purple circle marked with a cross. Black dots represent galaxies with measured distances. The large bold circle of radius 13.2° outlines the zero-velocity sphere (R_0 = 4.60 Mpc) around the Fornax-Eridanus cluster barycenter.

to the Fornax-Eridanus complex barycenter for both cases mentioned above, respectively.

The possible role of the barycenter position is illustrated by Fig. 6 representing velocity vs. distance diagrams where only the centers of the groups forming the Fornax-Eridanus complex are shown. The top panel represents radial velocities and distances of the groups relative to the Local Group centroid. The distance to the Fornax-Eridanus complex, 21.1 Mpc, corresponds to the spatial position of the complex barycenter as the weighted mean for position vectors of all the virialized substructures forming the complex. The displayed perturbations of the Hubble flow correspond to the mass of the whole Fornax-Eridanus complex estimated in this paper (2.16×10^{14} $M_\odot$) and the virial mass estimation of the Fornax cluster itself (0.87×10^{14} $M_\odot$; Makarov & Karachentsev 2011). Both sets include S-shaped lines signaling different angular separations from the complex center (0°, 5°, 15° and 30°). The error bars indicate rms uncertainties in distances and velocities.

The velocity vs. distance diagram relative to the center of the Fornax-Eridanus complex is shown in the bottom panel of Fig. 6. The displayed perturbations of the Hubble flow are caused by masses of 0.87×10^{14} $M_\odot$ (the virial mass estimation of the Fornax cluster itself), 0.53×10^{14} $M_\odot$, and 1.66×10^{14} $M_\odot$ (least square estimates for both adopted center positions mentioned above).

The structural complexity of the galaxy distribution suggests that probably the best mass indicator for this cluster should be based on the velocity field of the outskirt galaxies. Here two approaches are adopted. In the first, the radius of the zero velocity surface R_0 is estimated from a running median procedure. From the knowledge of R_0, the mass inside such a surface follows immediately. In the second, the expected radial velocity profile derived from the spherical model is fitted to the data, and again, the mass inside the zero-velocity surface results from the derived fit parameters.

3.2. The running median

The zero-velocity radius R_0 can be estimated from a running median procedure, using directly observational data (Fig. 7).

To account errors in observed distances and velocities and to give some estimates of the uncertainties, a Monte-Carlo simulation technique was used. For any galaxy i in a given dataset j, a corresponding distance from the center is generated according to the relation $R_i = R_{i,\text{obs}} + \Delta R_i \beta_{ij}$, where $R_{i,\text{obs}}$ is the observed distance from the Fornax center, ΔR_i is an observational error associated to the distance, and β_{ij} a normally distributed random number (with $\sigma = 1$). Generated velocities were derived by a similar procedure. About 10 000 datasets were generated and for each of them the running median method was applied, yielding different values of R_0, which were then averaged. The distributions of 10 000 R_0 are shown in Fig. 8, along with the mean and median values and the 90% error band (for the window w = 1 Mpc). The resulting median values and corresponding errors for (A) minor attractor and (B) major extended attractor cases are given in Table 3. The first two columns correspond to the cases where only precise or Tully-Fisher data were used for Monte-Carlo simulations, while the third column corresponds to the whole dataset. The lines of the table correspond to the different median windows.

With the Fornax cluster distance of ~20 Mpc and a typical uncertainty of 10% for the ACSFCS+ galaxies populating the central core of the cluster, the observational distance errors in the virialized zone will be about 2 Mpc. Assuming the virial radius of the Fornax cluster to be ~1.5 Mpc, we should conclude that the cluster core galaxies can possibly distort the pattern in the R_0 region for the Fornax cluster itself, but not for the whole Fornax-Eridanus complex. The galaxies in the Fornax cluster core, i.e. those with $R_{FC} < 3.5$–3.7 Mpc, were not regarded in the Monte-Carlo data simulations, resulting to 109 galaxies (see Fig. 7).

The substantial dip in the running median of simulations based on precise data can be explained partially by the enormous velocity of NGC 1400 (see, for example, Perrett et al. 1997). Belonging to the NGC 1407 group, NGC 1400 has extremely low velocity relative to the Local Group (558 km s^{-1}), while NGC 1407 has V_{LG} = 1771 km s^{-1}. Both galaxies have roughly the same distance (26.4 Mpc for NGC 1400 and 28.8 Mpc for NGC 1407 according to Tonry et al. 2001). In the velocity-distance diagrams NGC 1400 has a significant negative velocity relatively to the Fornax-Eridanus complex center, −380 km s^{-1} and −988 km s^{-1} for the cases of minor and major attractors respectively, and therefore it appears in the legend region at the Fornax-centric distance of 9.6 Mpc shifting the running median downwards.

According to the Table 3, the median estimate of R_0 is 4.60 Mpc with confidence interval corresponding to 90% error band of [3.88−5.60] Mpc. The mass inside the zero-velocity surface can be computed once R_0 is known. Using the spherical model, including the effects of the cosmological constant, the

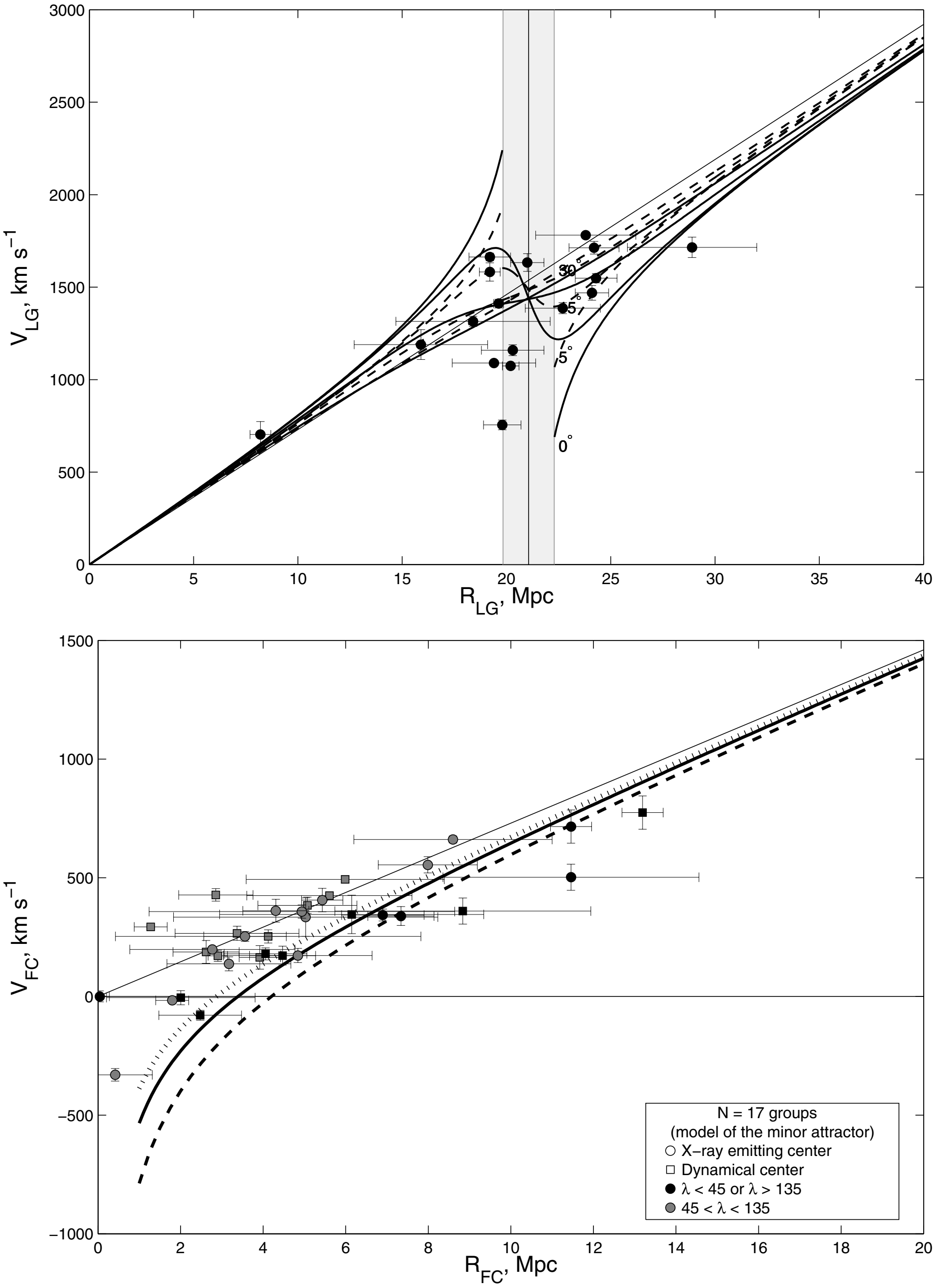

Fig. 6. *Top*: radial velocities and distances of the groups relative to the Local Group centroid. The distance to the Fornax-Eridanus complex, 21.1 Mpc, corresponds to the spatial position of the dynamical center of all substructures forming the complex. The sets of dashed and dotted lines indicate the Hubble flow perturbed by a point-like mass of 2.16×10^{14} $M_\odot$ and 0.87×10^{14} $M_\odot$ respectively, signing different angular separations from the complex center (0°, 5°, 15°, and 30°). The error bars indicate rms uncertainties in distances and velocities. *Bottom*: the velocity vs. distance diagram relative to the center of the Fornax-Eridanus complex. Round and square markers correspond to the center of the hot X-ray emitting gas and the dynamical center of all substructures forming the complex, respectively. The dotted, solid and dashed lines correspond to the Hubble flow perturbed by a point-like mass of 0.53×10^{14} $M_\odot$, 0.87×10^{14} $M_\odot$, and 1.66×10^{14} $M_\odot$, respectively.

Table 3. Radius R_0 and its 90% error band (in Mpc) obtained from Monte-Carlo simulations.

Window (Mpc)	Precise distances (samples 1–4)		TF distances (samples 5–6)		All samples	
	(A)	(B)	(A)	(B)	(A)	(B)
0.8	4.48	4.56	4.87	5.15	4.41	4.67
	3.88−5.46	3.94−5.63	3.95−6.18	4.08−6.68	3.83−5.39	3.93−5.76
1.0	4.58	4.72	5.04	5.39	4.42	4.78
	3.87−5.50	3.95−5.75	3.95−6.32	4.09−6.81	3.82−5.42	3.93−5.79
1.2	4.51	4.66	5.15	5.51	4.39	4.83
	3.88−5.56	3.92−5.85	3.95−6.33	4.16−6.86	3.82−5.48	3.93−5.88

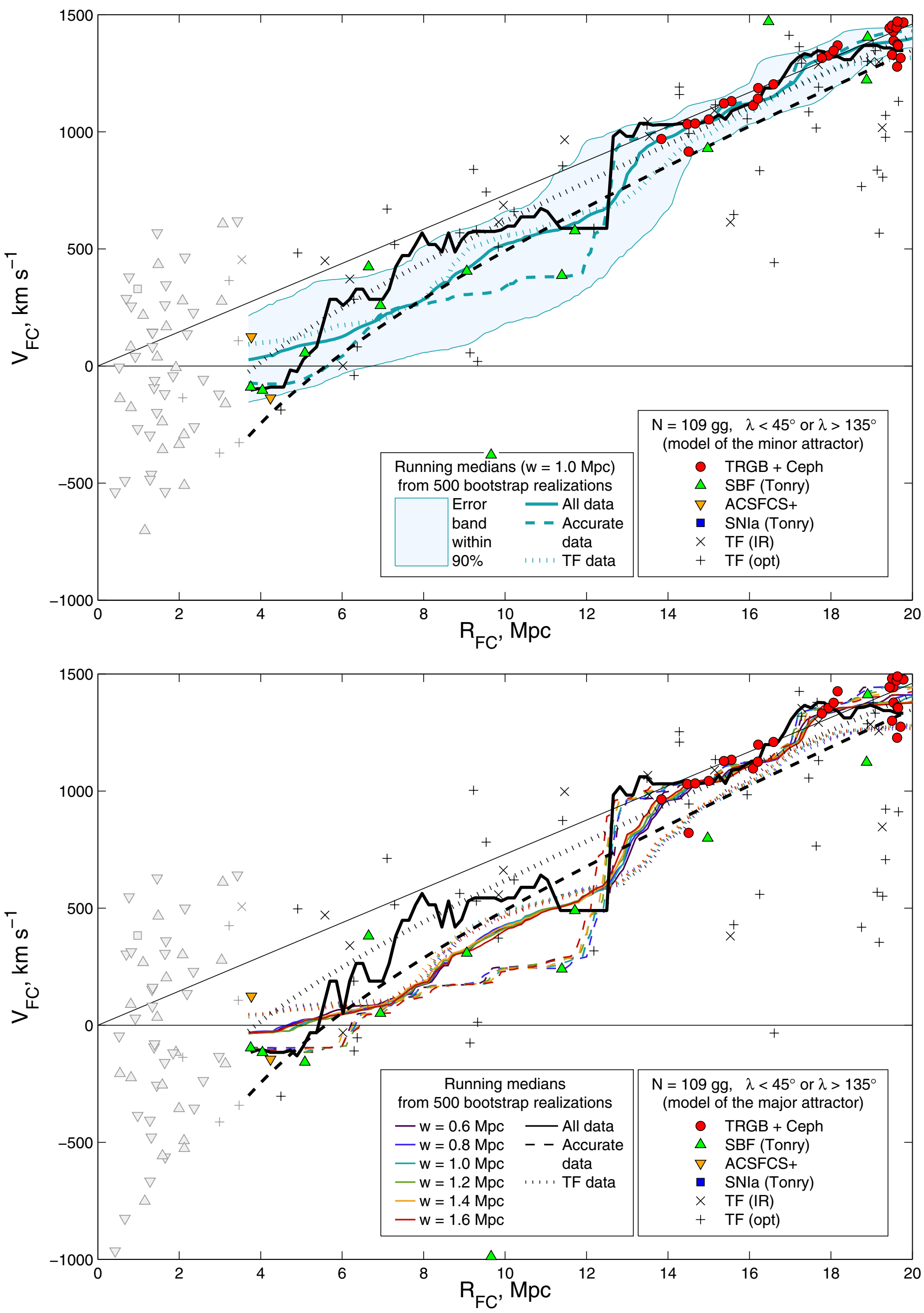

Fig. 7. Hubble flow in the Fornax cluster reference frame for 109 galaxies with $R_{FC} < 20$ Mpc. The black solid polygon curve traces the running median on observational data with a window of 1 Mpc. The dotted and dashed curves correspond to a Hubble flow perturbed by masses of $1.30 \times 10^{14}\ M_\odot$ and $3.93 \times 10^{14}\ M_\odot$, respectively, as the limiting cases within the confidence range. Only the galaxies with $\lambda < 45°$ or $\lambda > 135°$ are presented. *Top*: the case of almost pure Hubble flow ("minor attractor" approach). Blue curves trace the running medians on simulated data with a window of 1 Mpc and the corresponding 90% error band. *Bottom*: the case of almost pure infall towards the Fornax cluster ("major attractor" approach). Colored curves trace the running medians on simulated data with different window values.

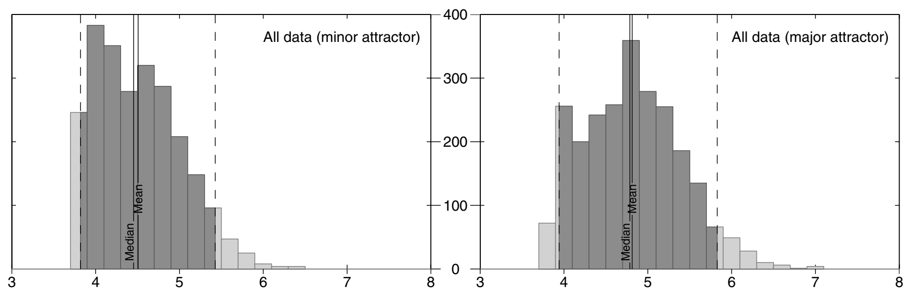

Fig. 8. Distribution of 10 000 R_0 realizations simulated using Monte-Carlo technique, their mean and median values, and the 90% error band. The window used for the running median procedure is $w = 1$ Mpc.

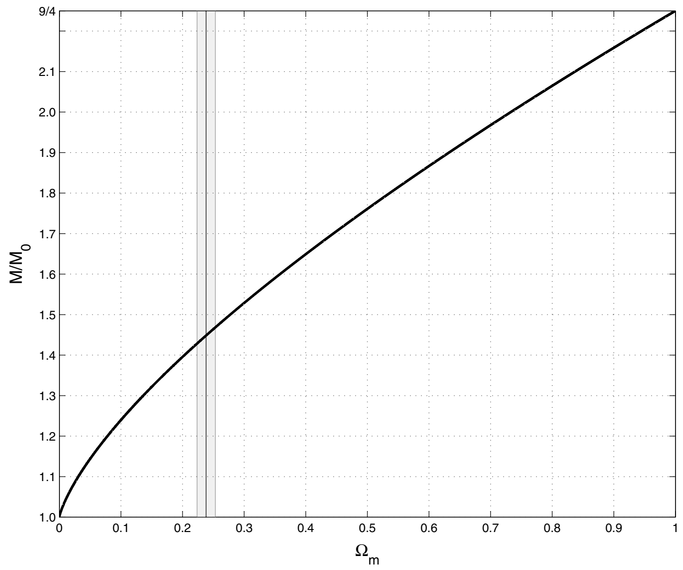

Fig. 9. Ratio of masses of a galaxy system computed in the ΛCDM model and in the empty Universe model respectively as a function of Ω_m. The value of $\Omega_m = 0.238 \pm 0.015$ adopted in the ΛCDM model is marked with a vertical gray strip.

mass inside R_0 is (Shaya, priv. comm.; Karachentsev et al. 2007)

$$M_T = \frac{\pi^2}{8G} R_0^3 \frac{H_0^2}{f^2(\Omega_m)} \tag{1}$$

where

$$f(\Omega_m) = \frac{1}{1-\Omega_m} - \frac{\Omega_m}{2(1-\Omega_m)^{3/2}} \mathrm{arccosh}\left(\frac{2}{\Omega_m} - 1\right), \tag{2}$$

with Ω_m the mass density parameter.

Figure 9 shows the ratio of masses of galaxy system computed in the ΛCDM model and in the empty Universe model as a function of Ω_m. As one can see, the adopted uncertainty in Λ value affects about 3% in mass estimation, which is negligible as compared with uncertainties caused by observational errors.

ΛCDM parameters can be determined from WMAP data with a sufficient accuracy; i.e., $H_0 = 73.2^{+3.1}_{-3.2}$ km s^{-1} Mpc^{-1} and $\Omega_m = 0.238 \pm 0.015$ (Spergel et al. 2007). Substituting these values into Eq. (1), we get

$$(M_T/M_\odot)_{0.24} = 2.23 \times 10^{12} (R_0/\mathrm{Mpc})^3. \tag{3}$$

From the numerical solution of the equations describing the Lemaître-Tolman model, modified to include effects of the cosmological constant, Peirani & de Freitas Pacheco (2008) obtain for the mass inside the zero-velocity surface

$$M = 4.24 \times 10^{12} h^2 R_0^3\, M_\odot. \tag{4}$$

The numerical coefficient was obtained for $\Omega_m = 0.3$, and for $h = 0.73$ both relations agree quite well when derived either analytically or numerically. For $R_0 = 4.60$ Mpc the corresponding total mass of the Fornax complex is $M = 2.16 \times 10^{14}\, M_\odot$, and for the limiting values of 90 % error band [3.88–5.60] Mpc we obtain $M = [1.30–3.93] \times 10^{14}\, M_\odot$ as a confidence interval.

Table 4. Masses resulting from the fit of Eq. (5) to the present data.

Parameter	"Minor attractor"	"Major attractor"
Mass (in $10^{14}\, M_\odot$)	0.93	1.55
	0.38−2.10	0.43−4.54
R_0 (in Mpc)	3.44	4.08
	2.57−4.52	2.67−5.85
σ (in km s^{-1})	300	345
σ_c (in km s^{-1})	84	190

3.3. Mass estimate from the radial velocity profile

In this section, the mass inside the zero-velocity surface is estimated by fitting a theoretical profile directly to data. We follow the procedure developed by Peirani & de Freitas Pacheco (2006, 2008), who have numerically computed the velocity field of outskirt galaxies, based on the spherical collapse model including effects of the cosmological constant. This approach assumes that a) most of the cluster mass is concentrated in the core, in which the shell crossing has already occurred, and b) that orbits of galaxies outside the core are mainly radial. From the numerical calculations by Peirani & de Freitas Pacheco (2008), the velocity-distance relation is

$$V(R) = 1.377 H_0 R - \frac{0.976 H_0}{R^n} \left(\frac{GM}{H_0^2}\right)^{(n+1)/3}. \tag{5}$$

Here M is the core cluster mass, R the distance of the member galaxy to the cluster center, $V(R)$ the radial velocity of the galaxy with respect to the mass center, H_0 the present value of the Hubble parameter and $n = 0.627$. The relation above results from a fit of numerical data and is valid for the present time ($z = 0$), since it varies as a function of the redshift. Equation (4) can be deduced from this equation when $V(R_0) = 0$.

In principle, if accurate radial velocities and distances are available, it is possible from the fitting of Eq. (5) to data to derive both the core cluster mass and the Hubble parameter (Peirani & de Freitas Pacheco 2008). Considering the uncertainties in the determination of Fornax-centric velocities, as explained in the previous section, we adopted the procedure of fixing H_0 as 73 km s^{-1} Mpc^{-1} and computing the mass either for the "minor attractor" or for the "major extended attractor" models.

Masses resulting from our fitting procedure are given in Table 4 for the two models adopted to estimate Fornax-centric velocities. The zero velocity surface radius R_0 and the velocity dispersion σ with respect to the mean infall flow are also given. The second column corresponds to velocities estimated from the "minor attractor" approach, whereas the third column gives values derived from the "major extended attractor" model. The corresponding confidence intervals for mass and R_0 values are estimated as a 90% error band. The third and the fourth lines give the uncorrected and the corrected velocity dispersions with respect to the infall flow towards Fornax, respectively. This method leads to values of masses that are, on the average, 50% lower than the "running median" approach, because it is a mass estimate for the Fornax cluster core than for the total Fornax-Eridanus complex. It is worth mentioning that the derived 1-D velocity dispersion with respect the bulk motion, (300–345 km s^{-1}), is one order of magnitude higher than observed in the vicinities of the Local Group, but it drops to (84–190 km s^{-1}) when the distance measurement errors are taken into account. Figure 10 shows the best fit between the expected velocity profile (Eq. (5)) derived from the spherical model and data, whose velocities were computed according to the "minor attractor" model (upper panel)

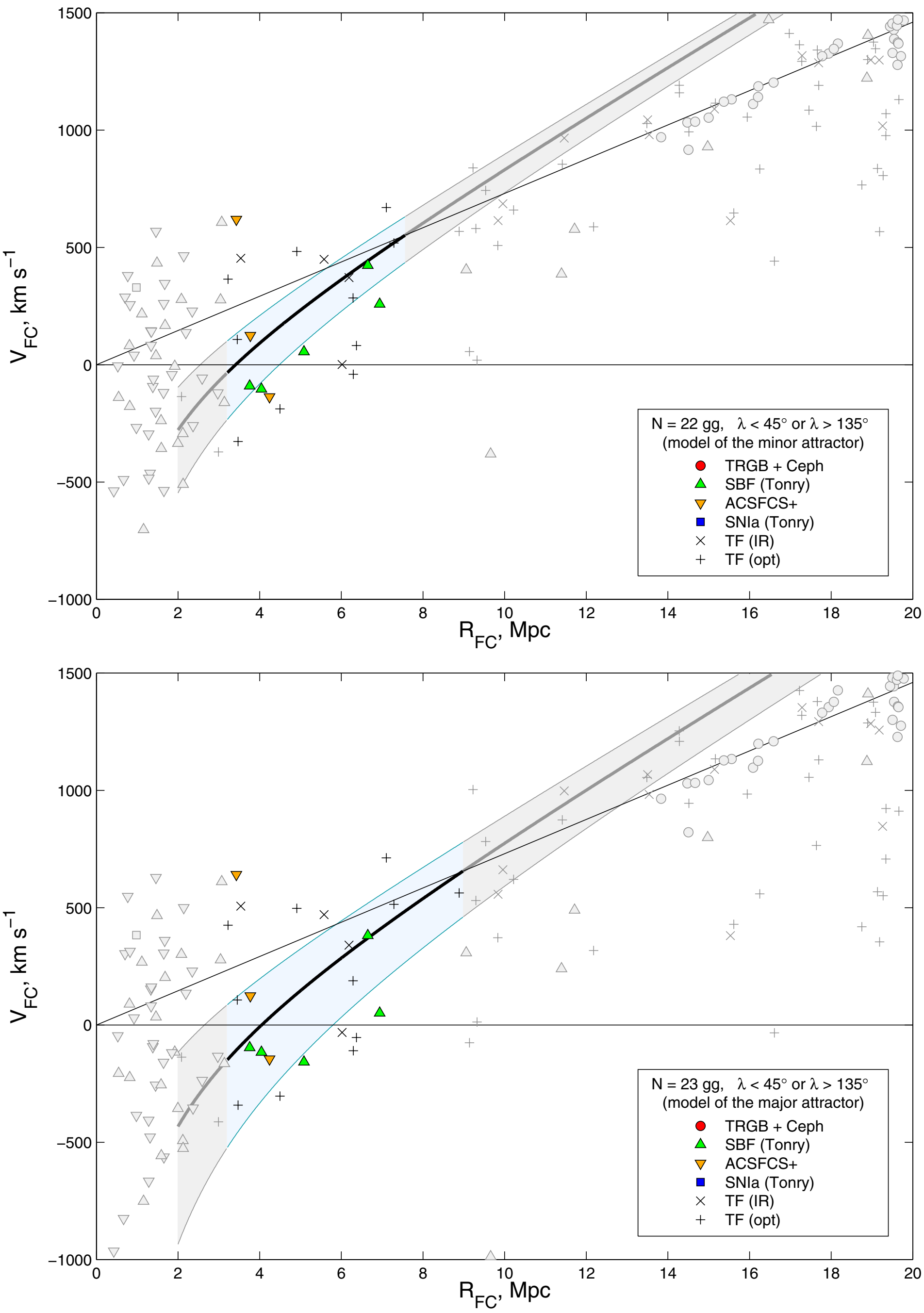

Fig. 10. Velocity field in the Fornax region, for 164 galaxies with distances less than 20 Mpc from the cluster center. The 90% error band resulting from Monte-Carlo simulations is shown. *Upper panel*: velocities derived according to the "minor attractor" approach. *Lower panel*: velocities derived according to the "major attractor" model.

or to the "major attractor" model (lower panel). The number of galaxies used in the fitting procedure is limited by $R_{\max}$ satisfying the relation $R_{\max}H_0 = V(R_{\max})$ and actually accounts for 22 and 23 galaxies, respectively.

Considering the mass values estimated from these procedures we adopt for the Fornax cluster itself a mass of $1.24 \times 10^{14}\ M_{\odot}$ with the confidence interval of $[0.40 - 3.32] \times 10^{14}\ M_{\odot}$, and a mass of $2.16 \times 10^{14}\ M_{\odot}$ for the total Fornax-Eridanus complex with the confidence interval of $[1.30 - 3.93] \times 10^{14}\ M_{\odot}$, which corresponds to a value that is half order of magnitude the Virgo cluster mass. In Table 5 we compare previous mass estimates for the Fornax cluster (normalized to $D_{\rm For} = 20$ Mpc and $D_{\rm Eri} = 25$ Mpc) with the present study, based on the velocity field of outskirt galaxies.

4. Concluding remarks

The distribution of galaxies in the vicinity of the Fornax cluster indicates a substantial degree of subclustering that is forming the Fornax complex. As a consequence, mass estimates based on the virial relation are affected by the fact that the system has not yet reached an equilibrium state and is still probably in formation (Dunn & Jerjen 2006). In fact, dwarf galaxies have distinct dynamic properties in comparison with bright galaxies and are

Table 5. Virial and total mass estimates (in 10^{14} $M_\odot$ units) for the Fornax-Eridanus complex.

Fornax	Eridanus	Other	Total	Ref.
1.53	0.20	0.15	1.88	1
1.15	0.70	–	1.85	2
–	0.7	–	–	3
1.00	0.92	–	1.92	4
0.87	0.62	0.43	1.92	5
0.40–3.32	–	–	–	6, Eq. (5)
–	–	–	1.30–3.93	6, via R_0

References. (1) Tully (1987); (2) Ferguson & Sandage (1990); (3) Brough et al. (2006); (4) Crook et al. (2007); (5) Makarov & Karachentsev (2011); (6) this paper.

probably falling into the system (Drinkwater et al. 2001). These difficulties may be circumvented by studying the velocity field of outskirt galaxies, which permits an estimate of the zero-velocity surface and, consequently, of the mass inside such a surface as originally proposed by Lynden-Bell (1981) and Sandage (1986).

In this investigation, a culled sample of 109 galaxies with measured distances and within 20 Mpc of the cluster center were used to study the velocity field in the neighborhood of the Fornax cluster. Since tangential velocities are unknown, two main assumptions were made in order to estimated the galaxy velocities with respect to the cluster center. In the first, it was supposed that the velocity vector is essentially dominated by the Hubble flow ("minor attractor" model), while in the second, it was assumed that galaxies are radially infalling ("major attractor" model). The zero-velocity radius was derived by two different methods: the "running median" and directly fits of the data to the expected velocity profile derived from the spherical model, including the effects of a cosmological constant.

The best fit radius of the zero-velocity sphere for the Fornax-Eridanus complex is estimated by us to be R_0 = 4.60 Mpc with the confidence interval of [3.38–5.60] Mpc, while the mass inside such a surface is $M_{\rm tot}$ = [1.30–3.93] × 10^{14} $M_\odot$. At the distance to Fornax cluster 20 Mpc, the radius R_0 = 4.60 Mpc corresponds to the 13.2° shown in Fig. 5. Within this circle there are almost all the systems identified by Makarov & Karachentsev (2011) as virialized groups bound to Fornax cluster. Their total virial mass, M = 1.92 × 10^{14} $M_\odot$, agrees with $M_{\rm tot}$, meaning that probably only a small part of the Fornax-Eridanus complex mass is spread between the groups.

Acknowledgements. Support for this work has been provided by Henri Poincaré Junior Fellowship of ADION in 2010, Observatoire de la Côte d'Azur, CNRS, France; the Dynasty Foundation of Noncommercial Programs, Russia; The Ministry of Education and Science of the Russian Federation (contract No. 14.740.11.0901); the Russian Foundation for Basic Research (projects No. 10-02-92650, 11-02-00639).

References

Biviano, A., Murante, G., Borgani, S., et al. 2006, A&A, 456, 23
Blakeslee, J. P., Jordán, A., Mei, S., et al. 2009, ApJ, 694, 556
Broadhurst, T. J., Taylor, A. N., & Peacock, J. A. 1995, ApJ, 438, 49
Brough, S., Forbes, D. A., Kilborn, V. A., et al. 2006, MNRAS, 369, 1351
Crook, A. C., Huchra, J. P., Martimbeau, N., et al. 2007, ApJ, 655, 790
Danese, L., de Zotti, G., Giuricin, G., et al. 1981, ApJ, 244, 777
Diaferio, A. 1999, MNRAS, 309, 610
Drinkwater, M. J., Gregg, M. D., Holman, B. A., & Brown, M. J. I. 2001, MNRAS, 326, 1076
Dunn, L. P., & Jerjen, H. 2006, AJ, 132, 1384
Evrard, A. E., Croton, D., White, M., Cohn, J., & Ellingson, E. 2006, BAAS, 38, 1196
Ferguson, H. C. 1989, AJ, 98, 367
Ferguson, H. C., & Sandage, A. 1990, AJ, 100, 1
Fernley, J. A., & Bhavsar, S. P. 1984, MNRAS, 210, 883
Girardi, M., & Biviano, A. 2002, in Merging Processes in Galaxy Clusters, ed. L. Ferreti, I. M. Gioia, & G. Giovannini (Dordrecht: Kluwer), 39
Haynes, M. P., Giovanelli, R., Salzer, J. J., et al. 1999 AJ, 117, 1668
Jerjen, H. 2003, A&A, 398, 63
Jones, C., Stern, C., Forman, W., et al. 1997, ApJ, 482, 143
Karachentsev, I. D., & Makarov, D. I. 1996, AJ, 111, 794
Karachentsev, I. D., & Kashibadze, O. G. 2006, Astrophysics, 49, 3
Karachentsev, I. D., & Makarov, D. I. 2008, AstBu, 63, 299
Karachentsev, I. D., & Nasonova, O. G. 2010, MNRAS, 405, 1075
Karachentsev, I. D., Sharina, M. E., Makarov, D. I., et al. 2002a, A&A, 389, 812
Karachentsev, I. D., Dolphin, A. E., Geisler, D., et al. 2002b, A&A, 383, 125
Karachentsev, I. D., Karachentseva, V. E., Huchtmeier, W. K., & Makarov, D. I. 2004, AJ, 127, 2031 (CNG)
Karachentsev, I. D., Dolphin, A. E., Tully, R. B., et al. 2006, AJ, 131, 1361
Karachentsev, I. D., Tully, R. B., Dolphin, A. E., et al. 2007, AJ, 133, 504
Karachentsev, I. D., Kashibadze, O. G., Makarov, D. I., & Tully, R. B. 2009, MNRAS, 393, 1265
Kashibadze, O. G. 2008, Astrophysics, 51, 409
Koribalski, B. S., Staveley-Smith, L., Kilborn, V. A., et al. 2004, AJ, 128, 16
Kudrya, Yu. N., Karachentseva, V. E., Karachentsev, I. D., et al. 2003, A&A, 407, 889
Lynden-Bell, D. 1981, The Observatory, 101, 111
Machacek, M., Dosaj, A., Forman, W., et al. 2005, ApJ, 621, 663
Makarov, D. I., & Karachentsev, I. D. 2009, AstBu, 64, 24
Makarov, D. I., & Karachentsev, I. D. 2011, MNRAS, submitted
Mellier, Y. 1999, ARA&A, 37, 127
Methewson, D. S., & Ford, V. L. 1996, ApJS, 107, 97
Metzler, C. A., White, M., Norman, M., & Loken, C. 1999, ApJ, 520, L9
Mitronova, S. N., Karachentsev, I. D., Karachentseva, V. E., Jarrett, T. H., & Kudrya, Yu. N. 2004, Bull. Spec. Astrophys. Obs., 57, 5 (2MFGC)
Peirani, S., & de Freitas Pacheco, J. A. 2006, New Astron., 11, 325
Peirani, S., & de Freitas Pacheco, J. A. 2008, A&A, 488, 845
Perea, J., del Olmo, A., & Moles, M. 1990, A&A, 237, 319
Perrett, K. M., Hanes, D. A., Butterworth, S. T., et al. 1997, AJ, 113, 895
Regos, E., & Geller, M. J. 1989, AJ, 98, 755
Reiprich, T. H., & Bohringer, H. 2002, ApJ, 567, 716
Rizzi, L., Tully, R. B., Makarov, D. I., et al. 2007, ApJ, 661, 813
Rosati, P., Borgani, S., & Norman, C. 2002, ARA&A, 40, 539
Sandage, A. 1986, ApJ, 307, 1
Sarazin, C. L. 1986, Rev. Mod. Phys., 58, 1
Scharf, C. A., Zurek, D. R., & Bureau, M. 2005, ApJ, 633, 154
Spergel, D. N., Bean, R., Doré, O., et al. 2007, ApJS, 170, 377
Springob, C. M., Haynes, M. P., Giovanelli, R., & Kent, B. R. 2005, ApJS, 160, 149
Springob, C. M., Masters, K. L., Haynes, M. P., et al. 2007, ApJS, 172, 599
Theureau, G., Martin, J. M., Cognard, L., et al. 2006, in ASP Conf. Ser., 351, ed. G. Gabriel, 429
Tifft, W. G., & Huchtmeier, W. K. 1990, A&AS, 84, 47
Tonry, J. L., Dressler, A., Blakeslee, J. P., et al. 2001, ApJ, 546, 681
Tonry, J. L., Schmidt, B. P., Barris, B., et al. 2003, ApJ, 594, 1
Tully, R. B. 1987, ApJ, 321, 280
Tully, R. B., & Pierce, M. J. 2000, ApJ, 533, 744
Tully, R. B., Rizzi, L., Dolphin, A. E., et al. 2006, AJ, 132, 729
Tully, R. B., Shaya, E. J., Karachentsev, I. D., et al. 2008, ApJ, 676, 184
Tully, R. B., Rizzi, L., Shaya, E. J., et al. 2009, AJ, 138, 323
Voit, G. M. 2005, Rev. Mod. Phys., 77, 207
Wu, X.-P. 2000, MNRAS, 316, 29